Using Redox-Active π Bridging Ligand as a Control Switch of Intramolecular Magnetic Interactions

Xiaozhou Ma, Elizaveta Suturina, Mathieu Rouzières, Mikhail Platunov, Fabrice Wilhelm, Andrei Rogalev, Rodolphe Clérac, Pierre Dechambenoit

Using Redox-Active π Bridging Ligand as a Control Switch of Intramolecular Magnetic Interactions

Xiaozhou Ma,[†,‡] Elizaveta A. Suturina,[#] Mathieu Rouzières,[†,‡] Mikhail Platunov,[⊥] Fabrice Wilhelm,[⊥] Andrei Rogalev,[⊥] Rodolphe Clérac,*[,†,‡] and Pierre Dechambenoit*[,†,‡]

[†] CNRS, CRPP, UMR 5031, Pessac F-33600, France

[‡] Univ. Bordeaux, CRPP, UMR 5031, Pessac F-33600, France

[#] Centre for Sustainable Chemical Technologies (CSCT), University of Bath, Claverton Down, Bath BA2 7AY, UK

[⊥] ESRF-The European Synchrotron, CS 40220, 38043 Grenoble Cedex 9, France

ABSTRACT: Intramolecular magnetic interactions in the dinuclear complexes $[(tpy)Ni(tphz)Ni(tpy)]^{n+}$ (n=4, 3 and 2; tpy: terpyridine; tphz: tetrapyridophenazine) were tailored by changing the oxidation state of the pyrazine-based bridging ligand. While its neutral form mediates a weak antiferromagnetic (AF) coupling between the two S=1 Ni(II), its reduced form, $tphz^{\bullet-}$, promotes a remarkably large ferromagnetic exchange of +214(5)K with Ni(II) spins. Reducing twice the bridging ligand affords weak Ni-Ni interactions, in marked contrast to the Co(II) analogue. Those experimental results, supported by a careful examination of the involved orbitals, provide a clear understanding of the factors which govern strength and sign of the magnetic exchange through an aromatic bridging ligand, a prerequisite for the rational design of strongly coupled molecular systems and high T_C molecule-based magnets.

The efficient control of the interactions between magnetic centers is a fascinating challenge, at the basis of any rational design of molecule-based magnets.[1] This fundamental problem is intrinsically linked to the question of the relative localization (or delocalization) of the unpaired electrons. Those are often located on *d* (or *f*) orbitals of metal ions, and interact weakly by superexchange through diamagnetic bridging ligands or atoms. Nevertheless, alternative strategies have received recently an increasing interest to promote strong magnetic coupling: (i) the mixed-valence approach, for which an electron delocalization promotes double-exchange, which exceeds superexchange;[2] and (ii) the radical bridge approach using an organic radical ligand acting as a magnetic relay between paramagnetic metal centers.[3] For the latter, the organic bridge characteristics are crucial to optimize the strength of the magnetic interactions: it should be strongly coordinating for an efficient mixing of the involved metal/organic orbitals,[3d,4] and its unpaired electron as delocalized as possible between the paramagnetic metal ions.

Based on these prerequisites, our group reported recently[4] a prototype dinuclear complex based on Co(II) and the redox-active tphz bridging ligand.[5] In this system, the intramolecular magnetic interactions are controlled by successive reduction processes. While the neutral form of tphz mediates a weak AF exchange between *ls*-Co(II) (*ls*: low-spin), the once reduced radical form stabilizes very strong AF couplings between the $S=^1/_2$ organic spin and the two *hs*-Co(II) (*hs*: high-spin). The resulting high-spin complex possesses a well isolated $S_T=^5/_2$ ground state that is remarkably the only thermally populated state at ambient temperature. When further reducing this dinuclear complex, despite the formal diamagnetic state of the $tphz^{2-}$ ligand, a strong AF coupling between two *hs*-Co(II) is observed, leading to an overall non-magnetic ground state. In this case, the strong magnetic interaction is induced by a large spin delocalization arising from an efficient orbital mixing of the $tphz^{2-}$ π system and one of the Co(II) singly-occupied *d* orbitals. Therefore, in this type of radical/metal ion complexes, the nature and magnitude of the intramolecular coupling is indeed predictable based on both electronic configurations of metal ions and the bridging ligand.

To further experimentally investigate the role of the metal/organic orbital complementarity in the control of the magnetic interactions, a novel family of dinuclear Ni(II) complexes was synthesized with the redox-active tphz ligand. The reaction of $Ni(tpy)Cl_2$,[6] $TlPF_6$ and tphz in CH_3CN leads to a new dinuclear nickel complex that was isolated as orange needle-shaped crystals of $[Ni_2(tphz)(tpy)_2](PF_6)_4 \bullet 3CH_3CN$ (**1**) after slow diffusion of Et_2O vapors (Supporting Information, SI). The single crystal X-ray diffraction data at 120K (Figure 1) reveal that **1** is isostructural to the Co(II) analogue,[5] possessing two equivalent $Ni^{II}(tpy)^{2+}$ fragments bridged by a neutral tphz ligand. The cyclic voltammetry of **1** in CH_3CN reveals four one-electron redox events at -0.40, -1.25, -1.66, -1.82V versus *vs.* Fc^+/Fc (Figure 2)[7] with a rest potential at -0.15V, indicating only reduction processes. By comparing with the reported Ru(II)[8] and Co(II)[4] analogues, the two processes at -0.40 and -1.25V can be assigned to the reduction of the bridging ligand and the other two most cathodic ones to the tpy reduction. The large separation between the two first redox potentials evidences the high stability of the tphz radical in the complex, with a comproportionation constant of *ca.* 2.6×10^{14}. Based on these redox properties, **1** was chemically reduced with KC_8 to give once and twice-reduced systems as $[Ni_2(tphz)(tpy)_2](PF_6)_3 \bullet 2Et_2O$ (**2**) and $[Ni_2(tphz)(tpy)_2](PF_6)_2 \bullet Et_2O$ (**3**) (SI) with similar coordination environments in the dinuclear cationic Ni(II) complexes (Figure S1, Table S1). Nevertheless, significant differences are seen when comparing the bond distances within the bridging ligand (Tables 1, S2)

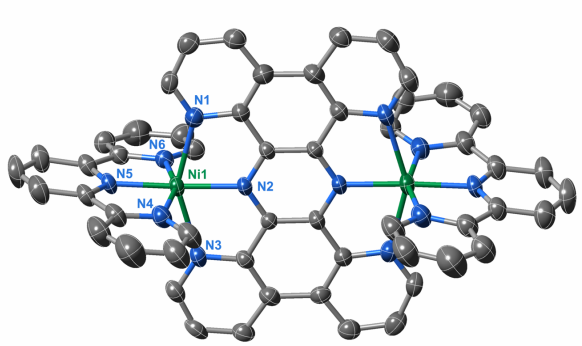

Figure 1. Crystal structure of $[Ni_2(tphz)(tpy)_2]^{4+}$ in **1** at 120K (thermal ellipsoids: 50%). H, solvents and anions are omitted for clarity.

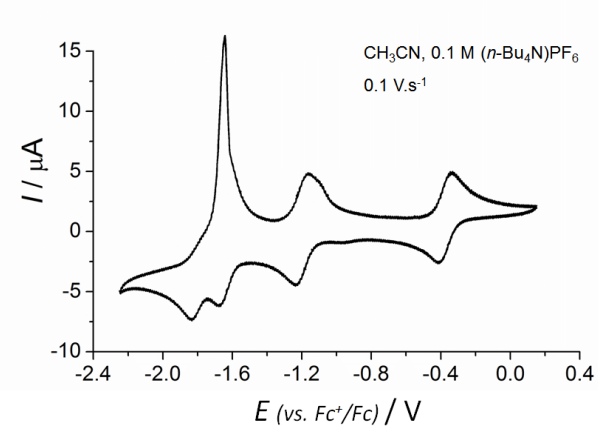

Figure 2. Cyclic voltammogram for a solution of **1**.

in agreement with two successive reductions as observed for the Co series.[4] In particular, C-N and N2⋯N2' distances in the tphz pyrazine ring are significantly elongated, highlighting the successive reductions mainly centered on the bridging ligand. The Ni1-N2 distance decreases from 1.980(4) to 1.921(4)Å upon the two reductions as a result of the increasing electrostatic interactions between the cationic metal and the bridging ligand. Those bond distances are particularly short, but in perfect agreement with the reported cobalt series.[4] The average Ni-N bond distance involving terpyridine remains quasi-unchanged upon these two first reductions, indicating the tpy redox innocence and that the Ni ion preserved its spin state and charge in agreement with CASSCF calculations (Figure S4).[9]

The local electronic and magnetic properties of the nickel metal ions were studied by X-ray absorption spectroscopy (XAS) and X-ray magnetic circular dichroism (XMCD). These techniques are particularly relevant for complexes with redox-active ligands, for which the oxidation state of the metal ion can be questioned.[10,11] The XAS spectrum at the Ni K-edge (Figure 3) is dominated by the $1s \rightarrow 4p$ transitions which show similar maxima for the three complexes between 8353.5 and 8353.8eV. As expected for comparable coordination sphere of the probed atom, the first EXAFS (Extended X-ray Absorption Fine Structure) oscillations overlap remarkably well. The much weaker pre-edge, dipole-forbidden, $1s \rightarrow 3d$ transitions are detected at 8335.9±0.2 and 8338.9±0.3eV for the three complexes in agreement with the expected and calculated Ni(II) ligand field splitting scheme (Figure S4).[11a] The XMCD experiments were also performed at the nickel K-edge to probe the Ni orbital magnetic moment (Figure 3). Considering that the spin–orbit interactions of the ligand atoms are negligibly small and thus cannot induce a significant orbital magnetic moment on the Ni centers, the observed XMCD signal at 8335.2±0.1eV is only due to the orbital polarization of the $4p$ and $3d$ states induced by the intra-atomic spin–orbit coupling of the Ni atoms. The Ni magnetic moment is thus directly proportional to the XMCD signals observed in the pre-edge and edge regions. Their quasi-identical intensities demonstrate the presence of the same magnetic moment and thus spin-state on the Ni metal ions in **1**, **2** and **3**. The similarity of the XAS and XMCD spectra establishes unambiguously the identical electronic and magnetic characteristics of the Ni site in these complexes.

To quantify the strength of the intramolecular magnetic coupling, dc magnetic measurements were performed at 0.1 T (Figure 4). The χT product of **1** remains constant between 300 and 80K at 2.4cm^{3}Kmol^{-1}, in good agreement with the presence of two S=1 Ni(II) (C_{Ni}=1.2cm^{3}Kmol^{-1}; g_{Ni}=2.19(5)). Below 80K, the progressive decrease of χT, to a minimum value of 0.38cm^{3}Kmol^{-1} at 1.85K, is the result of the concerted effect of weak AF interactions between nickel spins and the Ni magnetic anisotropy. The fit of the experimental data with both contributions (solid lines Figures 4, S8)[12,13] gives g_{Ni}=2.21(5), D_{Ni}/k_B=+13.6(3)K and $J_{Ni\text{-}Ni}/k_B$=-1.86(3)K comparable to -4.4K obtained by broken-symmetry DFT (B3LYP/def2-TZVP) calculations (SI).[9]

For the once-reduced analogue, **2**, the χT product at 300K is 4.1cm^{3}Kmol^{-1}, significantly higher than *ca.* 2.8cm^{3}Kmol^{-1} expected for one $S=^1/_2$ radical (g_{rad}=2.0) and two Ni(II) (g_{Ni}=2.2, S=1 in agreement with XAS/XMCD). This result suggests a remarkably strong ferromagnetic exchange between the metal ion and the bridging radical

Table 1. Selected bond distances (Å) in **1** – **3**.

	1	**2**	**3**
Ni-N1	2.268(5)	2.267(7)	2.305(4)
Ni-N2	1.980(4)	1.962(6)	1.921(4)
Ni-N3	2.336(5)	2.338(7)	2.326(4)
Ni-N4	2.089(5)	2.097(7)	2.100(4)
Ni-N5	1.975(4)	2.002(6)	1.997(3)
Ni-N6	2.078(5)	2.084(7)	2.114(4)
Ni-N(tpy)[b]	2.047(5)	2.061(7)	2.070(4)
C-C(pz)[a]	1.391(7)	1.384(10)	1.382(6)
C-N(pz)[a,b]	1.331(7)	1.359(9)	1.375(6)

[a] pz: pyrazine part of tphz; [b] average distance

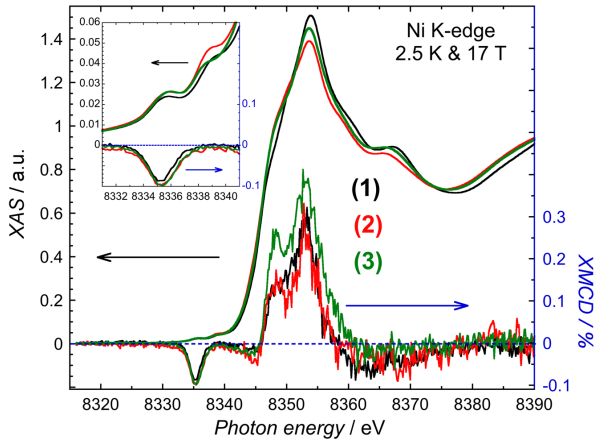

Figure 3. XAS and XMCD spectra. XAS spectra were normalized to zero before the edge and to unity far above the edge. XMCD spectra are given in XAS spectra %. Inset: magnification of the pre-edge region.

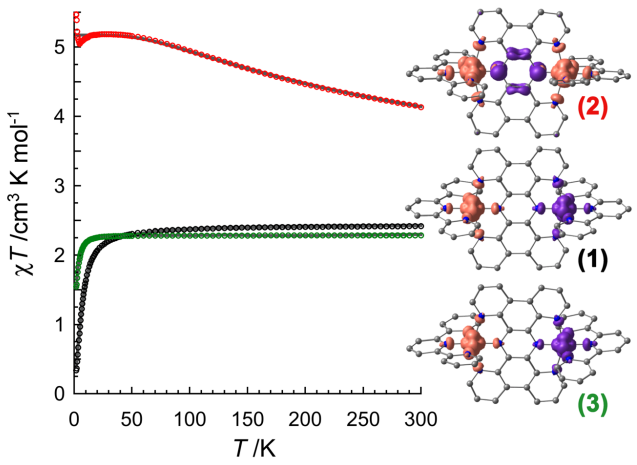

Figure 4. χT vs. T plot at 0.1T (gray lines: best fits; see text). Insets: Computed spin-density.

tphz$^{\bullet-}$ spins that is confirmed by the χT increase between 300 and 40K (Figures 4, S9). Below 40K, a χT plateau is reached with a maximum value of 5.2cm^{3}Kmol^{-1}, which corresponds to an $S_T=^5/_2$ ground state ($g_{S_T=5/2}$ = 2.18(5)). In this system, the ferromagnetic coupling is straightforward to rationalize considering the orthogonality of the Ni magnetic orbitals ($d_{x^2-y^2}$ and d_{z^2})[14] and the bridging ligand SOMO which is delocalized on the π system. Using an isotropic spin Heisenberg model,[15] its magnitude was estimated[13] to be $J_{Ni\text{-}rad}/k_B$=+214(5)K (g=2.17(5); Figure S9) leading to an energetically well isolated $S_T=^5/_2$ ground state (the first $S=^3/_2$ excited state lies at 214K above). This large coupling is in good agreement with the calculated one (+249K; DFT; SI),[9] and stronger than what was observed in other radical bridged Ni(II) complexes,[16] likely as a consequence of the strong metal-ligand coordination revealed by the short Ni-N2 bond.

For the twice-reduced compound **3**, the magnetic susceptibility data are similar to **1** with a constant χT product at *ca.* 2.3cm^{3}Kmol^{-1} between 300 and 25 K (Figures 4, S10), which is expected for a Curie behavior with two Ni(II) spins (g_{Ni}=2.14(5)). As suggested by structural and spectroscopic measurements, the magnetic properties conclude unambiguously that the Ni oxidation and spin states do not change after successive reductions. Upon cooling below 25K, the χT value decreases to 1.5cm^{3}Kmol^{-1} at 1.85K. Like in **1**, this low temperature behavior is probably the result of the combined contributions from the weak intramolecular AF interaction (-2.2K from DFT)[9] and the Ni magnetic anisotropy. The χT vs T and M vs H fits[12,13] lead systematically to $J_{Ni\text{-}Ni}$ values close to zero ($|J_{Ni\text{-}Ni}/k_B|$<0.1K) with g_{Ni}=2.14(5) and D_{Ni}/k_B=-10.4(3)K (solid lines in Figures 4, S10). Despite the presence of a significant magnetic anisotropy, no out-of-phase ac signal was detected above 1.85K and up to 10kHz for these compounds.

This new series of complexes with different redox states offers the appealing opportunity for a direct comparison between Ni(II) and Co(II) analogues, for which only the metal electronic configuration differs. Indeed, the once- and twice-reduced forms of the Ni and Co complexes are quasi-isometric, providing a unique platform to directly probe the influence of the singly-occupied atomic orbitals of the metal ion on the strength and sign of the magnetic coupling. According to the ab initio ligand field theory, the Ni(II) unpaired electrons are formally located on the $d_{x^2-y^2}$ and d_{z^2} orbitals (Figure S4),[14] which are only weakly interacting with tphz nitrogen σ-orbitals (Figures S5, S7). In this situation, the spin density is, as expected, mostly located on the metal ions in **1** and **3** (Figure 4) and the magnetic interactions between the two Ni(II) spins are necessarily weak. Moreover, those metal ion singly-occupied orbitals are orthogonal to the ligand π system. Therefore, as already mentioned, when the tphz$^{\bullet-}$ radical is stabilized in **2**, the unpaired electron is located on the ligand π orbital and a large ferromagnetic coupling is observed between metal and radical spins.

In *hs*-Co(II) analogues, in addition to the two unpaired electrons located on the $d_{x^2-y^2}$ and d_{z^2} orbitals, a third one is available on d_{xy}. This different configuration has a considerable impact on the magnetism,[4] as d_{xy} is the only orbital with an orientation that allows a significant overlap with the ligand π system. Hence, this efficient mixing of the d_{xy} and π orbitals induces an efficient spin density delocalization in the *hs*-Co(II) complexes. When twice-reduced, tphz^{2-} is formally diamagnetic, but the large spin delocalization promotes a strong AF coupling between the two Co(II) (-74K), in striking contrast to **3**.[17] This comparative study demonstrates the key role of the d_{xy} orbital on the strength of the intramolecular magnetic exchange.

At least one order of magnitude is also gained on the magnetic interaction, when a single electron is located on the ligand π orbital. The metal ion and tphz$^{\bullet-}$ spins are strongly ferromagnetically coupled in the Ni(II) case with J/k_B=+214K (*vide-supra*), while a huge antiferromagnetic exchange is observed for the *hs*-Co(II) complex (at least -500K). The $J(d_{xy}/\pi)$ coupling between the d_{xy} and π unpaired electrons is thus very large as it overcomes the ferromagnetic $J(d_{x^2-y^2}/\pi)$ and $J(d_{z^2}/\pi)$ contributions. Qualitatively, the $J(d_{xy}/\pi)$ interaction is thus larger than -700K from the simple $J_{co\text{-}rad}/k_B$–$J_{Ni\text{-}rad}/k_B$ relation.[18]

In conclusion, this work reports on a new series of dinuclear $[(tpy)Ni(tphz)Ni(tpy)]^{n+}$ complexes which provides, in comparison to the *hs*-Co(II) analogues, a complete set of experimental and theoretical results allowing a general understanding of the dominant factors governing the strength and nature of the magnetic coupling via an aromatic bridge. In particular, in addition to the obvious interest of using a radical bridging ligand, the careful selection of the metal ion based on its electronic configuration is the key step to promote the strongest possible coupling: this is happening when the unpaired electrons reside on the suitable t_{2g} orbitals, which overlap the best with the radical π system. This general approach should be easily transposed to systems with higher nuclearities and dimensionalities, for which strong magnetic exchanges could be fully exploited to design high temperature molecule-based magnets.[10,19]

■ ASSOCIATED CONTENT

Supporting Information

Experimental details about syntheses, structural, optical characterizations and theoretical calculations (PDF)
X-ray crystallographic data for **1**-**3** (CIF)

■ AUTHOR INFORMATION

Corresponding Authors

*dechambenoit@crpp-bordeaux.cnrs.fr
*clerac@crpp-bordeaux.cnrs.fr

ORCID

Elizaveta A. Suturina: 0000-0003-4407-1882
Rodolphe Clérac: 0000-0001-5429-7418
Pierre Dechambenoit: 0000-0001-7850-2260

■ ACKNOWLEDGMENTS

This work was supported by the ANR (ANR-16-CE29-0001-01, Active-Magnet project), the University of Bordeaux, the Région Nouvelle Aquitaine, the CNRS, the MOLSPIN COST action CA15128 and the Chinese Scholarship Council (CSC) for the PhD funding of XM. EAS thanks EPSRC for support (EP/N006895/1), the IRIDIS High Performance Computing Facility and associated services at the University of Southampton and RSC for travel grant. The authors thank also S. De, D. Woodruff, P. Perlepe, I. Oyarzabal and S. Exiga for their assistance and fruitful discussions as well as the GdR MCM-2.

■ REFERENCES

(1) (a) Verdaguer, M.; Bleuzen, A.; Marvaud, V.; Vaissermann, J.; Seuleiman, M.; Desplanches, C.; Scuiller, A.; Train, C.; Garde, R.; Gelly, G.; Lomenech, C.; Rosenman, I.; Veillet, P.; Cartier C.; Villain, F. Molecules to build solids: high T_C molecule-based magnets by design and recent revival of cyano complexes chemistry. *Coord. Chem. Rev.* **1999**, *190–192*, 1023-1047. (b) Weihe, H.; Güdel, H. U. Magnetic exchange across the cyanide bridge. *Comments Inorg. Chem.* **2000**, *22*, 75-103. (c) Ruiz E.; Rodriguez-Fortea, A.; Alvarez S.; Verdaguer, M. Is it possible to get high T_C magnets with Prussian blue analogues? A theoretical prospect. *Chem.–Eur. J.* **2005**, *11*, 2135-2144.

(2) (a) Bechlars, B.; D'Alessandro, D. M.; Jenkins, D. M.; Iavarone A. T.; Glover, S. D.; Kubiak, C.P.; Long, J. R. High-spin ground states via electron delocalization in mixed-valence imidazolate-bridged divanadium complexes. *Nat. Chem.* **2010**, *2*, 362-368. (b) Gaudette, A. I.; Jeon, I.-R.; Anderson, J. S.; Grandjean, F.; Long G. J.; Harris, T. D. Electron hopping through double-exchange coupling in a mixed-valence diiminobenzoquinone-Bridged Fe_2 Complex. *J. Am. Chem. Soc.* **2015**, *137*, 12617-12626.

(3) (a) Iwamura, H.; Inoue, K.; Hayamizu, T. High-spin polynitroxide radicals as versatile bridging ligands for transition metal complexes with high ferri/ferromagnetic T_C. *Pure & Appl. Chem.* **1996**, *68*, 243-252. (b) Rinehart, J. D.; Fang, M.; Evans, W. J.; Long, J. R. A N_2^{3-} radical-bridged terbium complex exhibiting magnetic hysteresis at 14 K. *J. Am. Chem. Soc.* **2011**, *133*, 14236-14239. (c) Fortier, S.; Le Roy, J. J.; Chen, C.-H.; Vieru, V.; Murugesu, M.; Chibobaru, L. F.; Mindiola, D. J.; Caulton, K. G. A dinuclear cobalt complex featuring unprecedented anodic and cathodic redox switches for single-molecule magnet activity. *J. Am. Chem. Soc.* **2013**, *135*, 14670-14678. (d) Jeon, I.-R.; Park, J. G.; Xiao, D. J.; Harris, T. D. An azophenine radical-bridged Fe_2 single-molecule magnet with record magnetic exchange coupling. *J. Am. Chem. Soc.* **2013**, *135*, 16845-16848. (e) Demir, S.; Nippe, M.; Gonzalez, M. I.; Long, J. R. Exchange coupling and magnetic blocking in dilanthanide complexes bridged by the multi-electron redox-active ligand 2,3,5,6-tetra(2-pyridyl)pyrazine. *Chem. Sci.* **2014**, *5*, 4701-4711. (f) DeGayner, J. A.; Jeon, I.-R.; Harris, T. D. A series of tetraazalene radical-bridged M_2 ($M = Cr^{III}, Mn^{II}, Fe^{II}, Co^{II}$) complexes with strong magnetic exchange coupling. *Chem. Sci.* **2015**, *6*, 6639-6648. (g) Demir, S.; Jeon, I.-R.; Long, J. R.; Harris, T. D. Radical ligand-containing single-molecule magnets. *Coord. Chem. Rev.* **2015**, *289*, 149-176. (h) Moilanen, J. O.; Chilton, N. F.; Day, B. M.; Pugh, T.; Layfield, R. A. Strong exchange coupling in a trimetallic radical-bridged cobalt(II)-hexaazatrinaphthylene complex. *Angew. Chem. Int. Ed.* **2016**, *55*, 5521-5525. (i) Wang, J.; Li, J.-N.; Zhang, S.-L.; Zhao, X.-H.; Shao, D.; Wang, X.-Y. Syntheses and magnetic properties of a pyrimidyl-substituted nitronyl nitroxide radical and its cobalt(II) complexes. *Chem. Commun.* **2016**, *52*, 5033-5036. (j) Dolinar, B. S.; Gómez-Coca, S.; Alexandropoulos, D. I.; Dunbar, K. R. An air stable radical-bridged dysprosium single molecule magnet and its neutral counterpart: redox switching of magnetic relaxation dynamics. *Chem. Commun.* **2017**, *53*, 2283-2286. (k) Gould, C. A.; Darago, L. E.; Gonzalez, M. I.; Demir, S.; Long, J. R. A trinuclear radical-bridged lanthanide single-molecule magnet. *Angew. Chem. Int. Ed.* **2017**, *56*, 10103-10107. (l) Demir, S.; Gonzalez, M. I.; Darago, L. E.; Evans, W. J.; Long, J. R. Giant coercivity and high magnetic blocking temperatures for N_2^{3-} radical-bridged dilanthanide complexes upon ligand dissociation. *Nat. Comm.* **2017**, *8*, 2144. (m) Dolinar, B. S.; Alexandropoulos, D. I.; Vignesh, K. R.; James, T. A.; Dunbar, K. R. Lanthanide triangles supported by radical bridging ligands. *J. Am. Chem. Soc.* **2018**, *140*, 908-911. (n) Lemes, M. A.; Stein, H. N.; Gabidullin, B.; Robeyns, K.; Clérac, R.; Murugesu, M. Probing magnetic-exchange coupling in supramolecular squares based on reducible tetrazine-derived ligands. *Chem. Eur. J.* **2018**, *24*, 4259-4253.

(4) Ma, X.; Suturina, E. A.; De, S.; Négrier, P.; Rouzières, M.; Clérac, R.; Dechambenoit, P. A redox-active bridging ligand to promote spin delocalization, high-spin complexes, and magnetic multi-switchability. *Angew. Chem. Int. Ed.* **2018**, *57*, 7841-7845.

(5) Iwamura, H.; Koga, N. Molecular approaches to photomagnetic materials. Metal-dependent regiospecificity in the exchange coupling of magnetic metal ions with free radical substituents on pyridine base ligands. *Pure & Appl. Chem.* **1999**, *71*, 2, 231-238.

(6) Lions, F.; Dance, I. G.; Lewis, J. Mono-chelate complexes of pyridine-2-aldehyde 2'-pyridylhydrazone. *J. Chem. Soc. A*, **1967**, 565-572.

(7) The one electron process was confirmed by measuring the rest potential of solutions of **1** and **2**, respectively 0 V and -0.7 V, prior recording the cyclic voltammograms which were found to be identical.

(8) (a) Bonhôte, P.; Lecas, A.; Amouyal, E. Bi-and tri-nuclear ruthenium(II) complexes containing tetrapyridophenazine as a rigid bridging ligand. *Chem. Commun.* **1998**, *8*, 885-886. (b) Gourdon, A.; Launay, J.-P. Mononuclear and binuclear tetrapyrido[2,3-a:3',2'-c:2",3"-h:3"',2"'-j]phenazine (tphz) ruthenium complexes. *Inorg. Chem.* **1998**, *37*, 5336-5341.

(9) Neese, F. The ORCA program system. *WIREs Comput. Mol. Sci.* **2012**, *2*, 73-78.

(10) Pedersen, K. S.; Perlepe, P.; Aubrey, M. L.; Woodruff, D. N.; Reyes-Lillo, S. E.; Reinholdt, A.; Voigt, L.; Li, Z.; Borup, K.; Rouzières, M.; Samohvalov, D.; Wilhelm, F.; Rogalev, A.; Neaton, J. B., Long, J. R.; Clérac, R. Formation of the layered conductive magnet $CrCl_2(pyrazine)_2$ through redox-active coordination chemistry. *Nat. Chem.* **2018**, *10*, 1056-1061.

(11) (a) Pickering, I. J.; George, G. N.; Lewandowski, J. T.; Jacobson, A. J. Nickel K-edge X-ray absorption fine structure of lithium nickel oxides. *J. Am. Chem. Soc.* **1993**, *115*, 4137-4144. (b) Szilagyi, R. K.; Lim, B. S.; Glaser, T.; Holm, R. H.; Hedman, B.; Hodgson, K. O.; Solomon, E. I. Description of the ground state wave functions of Ni dithiolenes using sulfur K-edge X-ray absorption spectroscopy. *J. Am. Chem. Soc.* **2003**, *125*, 9158-9169. (c) Perlepe, P.; Oyarzabal, I.; Pedersen, K.S.; Negrier, P.; Mondieig, D.; Rouzières, M.; Hillard, E.A.; Wilhelm, F.; Rogalev, A.; Suturina, E.A.; Mathonière C.; Clérac, R. $Cr(pyrazine)_2(OSO_2CH_3)_2$: a two-dimensional coordination polymer with an antiferromagnetic ground state. *Polyhedron* **2018**, *153*, 248-253. (d) Liang, H. W.; Kroll, T.; Nordlund, D.; Weng, T.-C.; Sokaras, D.; Pierpont, C. G.; Gaffney K. J. Charge and spin-state characterization of cobalt bis(o-dioxolene) valence tautomers using Co Kβ X-ray emission and L-Edge X-ray absorption spectroscopies. *Inorg. Chem.* **2017**, *56*, 737-747. (e) Koroidov, S.; Hong, K.; Kjaer, K. S.; Li, L.; Kunnus, K.; Reinhard, M.; Hartsock, R. W.; Amit, D.; Eisenberg, R.; Pemmaraju, C.D.; Gaffney, K.; Cordones, A. A. Probing the electron accepting orbitals of Ni-centered hydrogen evolution catalysts with noninnocent ligands by Ni L-edge and S K-edge X-ray absorption. *Inorg. Chem.* **2018**, *57*, 13167-13175. (f) Jafri, S. F.; Koumousi, E. S.; Arrio, M.-A.; Juhin, A.; Mitcov, D.; Rouzières, M.; Dechambenoit, P.; Li, D.; Otero, E.; Wilhelm, F.; Rogalev, A.; Joly, L.; Kappler, J.-P.; Moulin, C. C. D.; Mathonière, C.; Clérac, R.; Sainctavit, P. Atomic scale evidence of the switching mechanism in a photomagnetic CoFe dinuclear Prussian blue analogue. *J. Am. Chem. Soc.* **2019**, *141*, 3470-3479.

(12) The following Hamiltonian has been used to fit the magnetic data:
$\hat{H} = -2J_{Ni-Ni}(\vec{S}_{Ni1} \cdot \vec{S}_{Ni2}) + 2D_{Ni}S^2_{Ni,z} + 2g_{Ni}\mu_B\vec{S}_{Ni} \cdot \vec{H}$

(13) Chilton, N. F.; Anderson, R. P.; Turner, L. D.; Soncini, A.; Murray, K. S. PHI: a powerful new program for the analysis of anisotropic monomeric and exchange-coupled polynuclear d- and f-block complexes. *J. Comput. Chem.* **2013**, *34*, 1164-1175.

(14) The average N1-Ni-N3 axis is taken as the z direction by convention (Figure 1).

(15) The following Hamiltonian has been used to fit the magnetic data:
$\hat{H} = -2J_{Ni-rad}(\vec{S}_{Ni1} + \vec{S}_{Ni2}) \cdot \vec{S}_{rad} + \mu_B(2g_{Ni}\vec{S}_{Ni} + g_{rad}\vec{S}_{rad}) \cdot \vec{H}$

(16) (a) Dei, A.; Gatteschi, D.; Pardi, L. Sextet ground state in a dinuclear nickel(II) complex containing a tetraoxolene radical as bridging ligand. *Inorg. Chim. Acta* **1991**, *189*, 125-128. (b) Woods, T. J.; Stout, H. D.; Dolinar, B. S.; Vignesh, K. R.; Ballesteros-Rivas, M. F.; Achim, C.; Dunbar, K. R. Strong ferromagnetic exchange coupling mediated by a bridging tetrazine radical in a dinuclear nickel complex. *Inorg. Chem.* **2017**, *56*, 12094-12097. (c) Lemes, M. A.; Brunet, G.; Pialat, A.; Ungur, L.; Korobkova, I.; Korobkov, I.; Murugesu, M. Strong ferromagnetic exchange coupling in a $\{Ni^{II}_4\}$ cluster mediated through an air-stable tetrazine-based radical anion. *Chem. Commun.* **2017**, *53*, 8660-8663.

(17) This is further confirmed by UV-vis-NIR spectrometry which reveals the absence of an absorption band in the NIR region for **3** (Figure S3) in contrast to its Co analogue (reference 4).

(18) More accurately, this $J(d_{xy}/\pi)$ antiferromagnetic coupling is better described as being between the d_{xy}(Co)+π(N_{tphz}) orbital and the π system of the carbon atoms of the tphz pyrazine part (for symmetry reasons of the involved orbitals).

(19) (a) Manriquez, J. M.; Yee, G. T.; McLean, R. S.; Epstein, A. J.; Miller, J. S. A room-temperature molecular/organic-based magnet. *Science* **1991**, *252*, 1415-1417. (b) Miller J. S. Magnetically ordered molecule-based materials. *Chem. Soc. Rev.* **2011**, *40*, 3266-3296. (c) Miller J. S., Ohkoshi, S.-i. in *High-T_C Ordered Molecular Magnets in* Molecular Magnetic Materials: Concepts and Applications; Eds. Sieklucka, B.; Pinkowicz, D., Wiley–VCH: Wienheim, 2017.

Table of Content Artwork

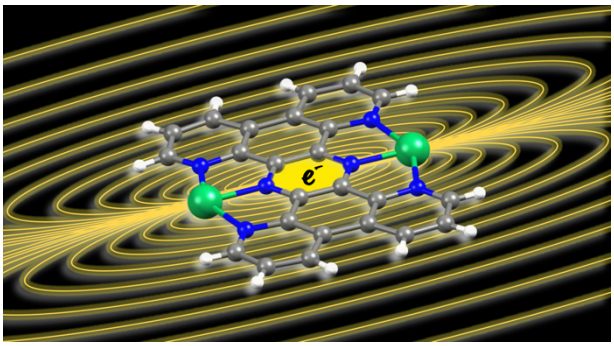

Supplementary Information for

Using Redox-Active π Bridging Ligand as a Control Switch of Intramolecular Magnetic Interactions

Xiaozhou Ma,[a,b] Elizaveta A. Suturina,[c] Mathieu Rouzières,[a,b] Mikhail Platunov,[d] Fabrice Wihelm,[d] Andrei Rogalev,[d] Rodolphe Clérac,*[a,b] and Pierre Dechambenoit*[a,b]

[a] CNRS, CRPP, UMR 5031, Pessac F-33600, France

[b] Univ. Bordeaux, CRPP, UMR 5031, Pessac F-33600, France

[c] Centre for Sustainable Chemical Technologies (CSCT), University of Bath, Claverton Down, Bath BA2 7AY, UK

[d] ESRF-The European Synchrotron, CS 40220, 38043 Grenoble Cedex 9, France

Email : dechambenoit@crpp-bordeaux.cnrs.fr
clerac@crpp-bordeaux.cnrs.fr

1. Experimental and synthetic methods

a. Experimental technics

Elemental analyses (EA) were performed on a ThermoFischer Flash EA 1112.
FT-IR spectra were recorded on a Thermal Scientific Nicolet^{TM} 6700 ATR (attenuated total reflection) spectrometer equipped with a Smart iTR diamond window.
Electrochemistry: Cyclic voltammetry (CV) measurements were performed for compounds **1** and **2** with a Metrohm Autolab PGSTAT101 equipped with a platinum working electrode. Ferrocene was used as an internal reference. Measurements were done in CH_3CN with 0.1 M (n-Bu_4N)PF_6 as supporting electrolyte, at a scan rate of 0.1 V/s. As expected, the CV of **1** and **2** were found to be exactly the same, just the rest potential was different (-0.15 V for **1** and -0.68 V for **2**), confirming the one electron reduction process at -0.4 V.
UV-vis-NIR spectra were recorded using a Perkin Elmer LAMBDA 950 in dry acetonitrile.
Crystallographic data were collected with a Bruker APEX II Quasar diffractometer, equipped with a graphite monochromator centred on the path of MoK_α radiation (λ = 0.71073 Å). The single crystals were coated with Cargille^{TM} NHV immersion oil and mounted on a fiber loop, followed by data collection at 120 K. The program SAINT was used to integrate the data, which was thereafter corrected using SADABS.[1] The structures were solved using direct methods and refined by a full-matrix least-squares method on F^2 using SHELXL-2014.[2] All non-hydrogen atoms were refined with anisotropic displacement parameters. Hydrogen atoms were assigned to ideal positions and refined isotropically using a riding model.
For compound **1**, one of the two crystallographic acetonitrile molecules was found to be disordered over two positions with equal occupancies. Hydrogen atoms on this disordered acetonitrile molecule were not introduced, but are considered in the formula.
For compound **2**, all the tested crystals were very small and weakly diffracting, thus the data were cut at 1.0 Å as there is no reflection above. This experimental limitation results in a low data/parameters ratio. The Et_2O molecule was found to be disordered over two positions and refined using SADI, SIMU, EADP and EXYZ restraints and constraints.
For compound **3**, disordered Et_2O molecules are also present, but the disorder cannot be modeled correctly without using too many restraints or constraints. Therefore, those were treated as a diffuse contribution to the overall scattering without specific atom positions using the SQUEEZE procedure in PLATON.[3]
The crystallographic data for **1- 3** are listed in Table S1. The CIF files have been deposited at the Cambridge Crystallographic Data Centre as supplementary publication no. CCDC 1861535-1861537.
X-ray absorption spectroscopy. XAS and XMCD spectra were obtained at the ID12 beamline (ESRF – The European Synchrotron) on pressed pellets of polycrystalline samples of **1**, **2** and **3**. We used fundamental harmonic of Apple-II type undulator for experiments at the Ni K-edge. All XAS spectra were recorded using total fluorescence yield detection mode and were subsequently corrected for reabsorption effects. The XMCD spectra were obtained as the difference between two consecutive XAS spectra recorded with opposite photon helicities. Furthermore, the XMCD spectra were systematically obtained in both magnetic field directions (at 17 T) in order to ensure the absence of experimental artifacts.
Magnetic susceptibility measurements were performed on a Quantum Design SQUID

magnetometer MPMS-XL and PPMS-9 Quantum Design susceptometer at temperatures between 1.8 and 400 K and dc magnetic fields ranging from -7 to 7 T. Measurements were performed on a finely crystalline sample of **1**, **2** and **3** (13.76 mg, 6.6 & 24.9 mg, 12.1 & 2.0 mg respectively) sealed in a polypropylene bag (3 × 0.5 × 0.2 cm: 19.75 mg for **1**, 18.8 & 24.4 mg for **2**, 21.4 & 31.4 mg for **3**) with oil (17.02 mg for **1**, 16.2 & 14.1 mg for **2**, without for **3**) to avoid the orientation of the sample when necessary. Prior to the experiments, the field dependent magnetization was measured at 100 K in order to detect the presence of any bulk ferromagnetic impurities. The samples appeared to be free of any significant ferromagnetic impurities. The magnetic data were corrected for the sample holder, oil and the intrinsic diamagnetic contributions.

DFT and CASSCF calculations have been carried out using ORCA 4.0 program[4] package and the crystal structure of the molecules. Energies and corresponding spin densities have been computed with B3LYP functional and def2-TZVP basis set for various spin states corresponding to *hs* or *ls* Ni(II) site. Ab initio ligand field calculations[5] have been done with CASSCF(8,5)/def2-TZVP for 10 triplet and 15 singlet states of modified structures where one of the Ni(II) ions have been replaced with a Zn(II) center. Spin-Hamiltonian parameters, *D* and *g*, have been computed using the mean field spin-orbit coupling approximation.[6]

b. Syntheses

Tetrapyridophenazine (tphz - Scheme S1),[7,8,9] Ni(tpy)Cl_2[10] and KC_8 were prepared using procedures described in the literature. Reactions for the syntheses of complexes **2** and **3** were carried out under a dry nitrogen atmosphere using a glovebox. Diethyl ether (Et_2O), acetonitrile (CH_3CN) and tetrahydrofuran (THF) were purified using an Innovative Technologies solvent purification system.

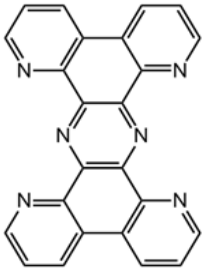

Scheme S1. Structure of tphz.

Synthesis of [Ni_2(tphz)(tpy)$_2$](PF_6)$_4$•3MeCN (1). 188 mg (0.521 mmol; 1.0 eq) of Ni(tpy)Cl_2, 100 mg (0.257 mmol; 0.49 eq.) of tphz and 364 mg (1.05 mmol; 2.0 eq.) of $TlPF_6$ were reacted in 20 mL of CH_3CN for 10 hours, the resulting orange solution was filtrated through using plastic VWR filter. Orange crystals came out from diethyl ether diffusion into the solution with an approx. 90 % yield based on Ni. TGA: 26-250°C: -7.3 % (calcd -7.3 % for 3 CH_3CN); decomp.> 270°C. Elemental analysis found (calcd) for $C_{60}H_{43}Ni_2F_{24}N_{15}P_4$: C 42.70(43.12), H 2.83(2.59) N 12.58(12.57). IR of **1** (solid, $\bar{\nu}$/cm^{-1}) 649(m), 669(m), 704 (s), 734 (s), 768 (vs), 823 (vs), 1017(s), 1039 (w), 1099 (w), 1162 (w), 1187 (w), 1213 (w), 1251 (w), 1326 (s), 1387 (m), 1414(m), 1453 (m), 1475 (m), 1506 (w), 1533 (w), 1560 (w), 1581 (w), 1604 (w), 2251 (w).

Synthesis of [Ni_2(tphz)(tpy)$_2$](PF_6)$_3$•2Et_2O (2). Compound **1** (50 mg; 0.030 mmol) and 4.5 mg of KC_8 (0.033 mmol; 1.1 eq.) were stirred in 3 mL of THF at room temperature for 4 hours and filtered with a Sartorius filter. The solid was dissolved in CH_3CN and filtered using plastic VWR filter (porosity 0.2 µm). Dark brown crystals were obtained from slow diffusion of diethyl ether with an approx. 42 % yield based on Ni. TGA: decomp.> 350° C. Elemental analysis found (calcd) for $C_{62}H_{54}Ni_2F_{18}N_{12}P_3O_2$: C 47.64(48.00), H 3.53(3.51) N 10.63(10.83). IR of **2** (solid, $\bar{\nu}$/cm^{-1}) 643 (m), 650 (m), 668(m), 699 (s), 740 (s), 765 (vs), 789(s), 822 (vs), 899 (w), 996 (w), 1018 (m), 1035 (w), 1106 (w), 1165 (w), 1187 (w), 1205 (m), 1250 (w), 1320 (m), 1357 (s), 1400 (w), 1445 (m), 1474 (m), 1505 (m), 1580 (w), 1602 (w), 1979 (w).

Synthesis of $[Ni_2(tphz)(tpy)_2](PF_6)_2 \cdot Et_2O$ (3). Compound **1** (30 mg; 0.018 mmol) and 5.6 mg of KC_8 (0.041 mmol; 2.3 eq.) were stirred in 2.5 mL of THF at room temperature for 6 hours and filtered with a Sartorius filter. The solid was dissolved in DMF and filtered using plastic VWR filter (porosity 0.2 µm). Black crystals were obtained from slow diffusion of diethyl ether with an approx. 18 % yield based on Ni. TGA: 25-140°C: -6.0 % (calcd -5.6 % for Et_2O); decomp.> 380°C. Elemental analysis found (calcd) for $C_{58}H_{44}Ni_2F_{12}N_{12}P_2O$: C 51.66(52.28), H 3.98(3.33) N 11.89(12.62). IR of **3** (solid, $\bar{\nu}/cm^{-1}$) 640 (s), 650 (m), 665 (m), 729 (s), 748 (s), 767(vs), 822 (vs), 876 (w), 987 (m), 1016 (m), 1032 (m), 1044 (m), 1069 (w), 1080(w), 1108(m), 1165 (m), 1183 (s), 1249 (m), 1319 (s), 1345 (s), 1389 (m), 1428 (m), 1447 (s), 1489 (s), 1549 (s), 1588 (m), 1666(w), 2167 (w), 2860 (w).

2. Crystallographic Studies

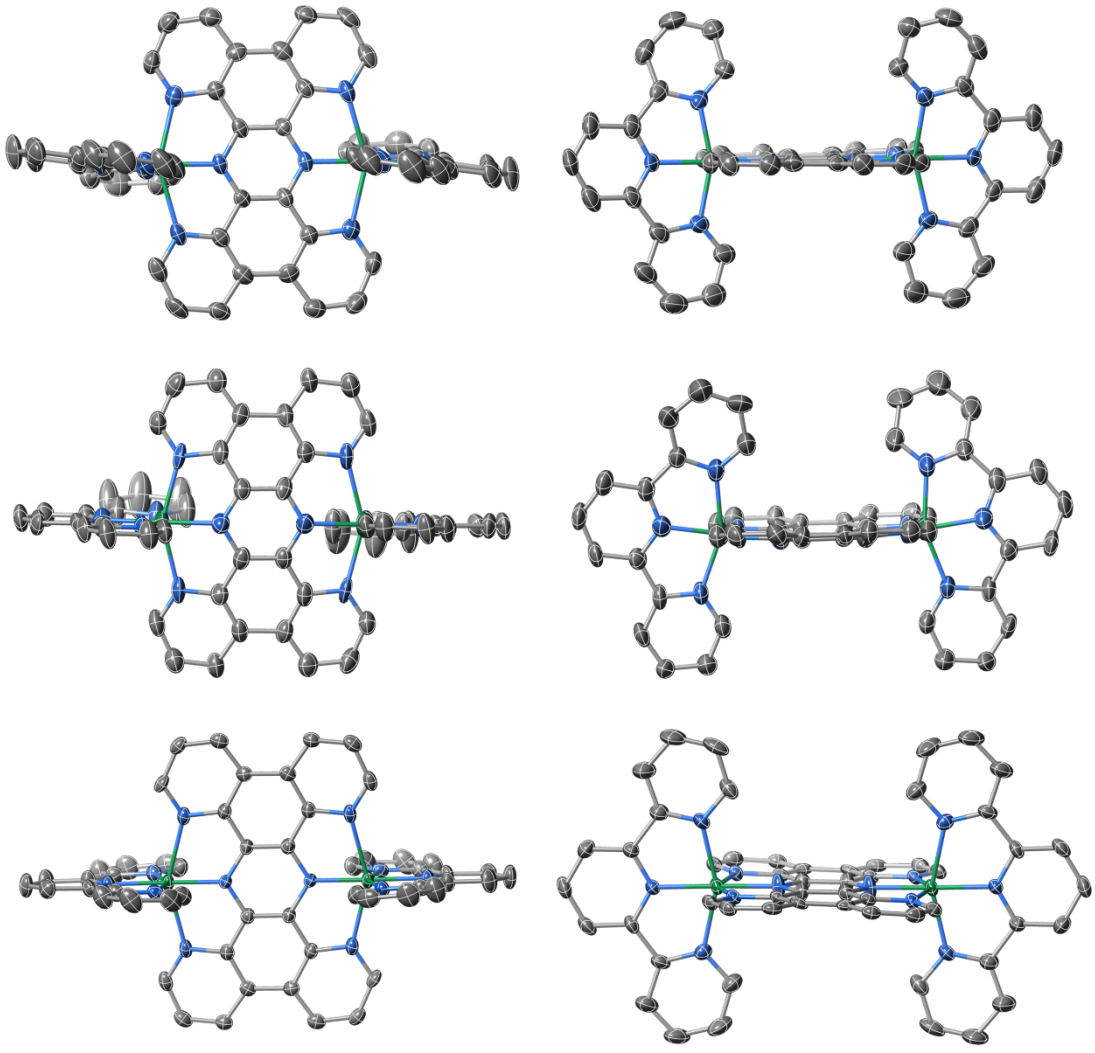

Figure S1. Two perpendicular ORTEP-type views (left and right) of the cationic complexes in **1** (top), **2** (middle) and **3** (bottom) (C grey, Ni green, N blue) at 120 K. Thermal ellipsoids are depicted at a 50 % probability level. Hydrogen atoms are omitted for clarity.

Table S1. Crystal data and structure refinements.

Compound	$[Ni_2(tphz)(tpy)_2](PF_6)_4$ •$3CH_3CN$ **(1)**	$[Ni_2(tphz)(tpy)_2](PF_6)_3$ •$2Et_2O$ **(2)**	$[Ni_2(tphz)(tpy)_2](PF_6)_2$ •Et_2O **(3)**
Formula	$Ni_2C_{60}H_{43}N_{15}P_4F_{24}$	$Ni_2C_{62}H_{54}N_{12}O_2P_3F_{18}$	$C_{58}H_{44}N_{12}Ni_2OP_2F_{12}$
FW ($g \cdot mol^{-1}$)	1671.39	1551.50	1332.41
Crystal color	orange	brown	black
Crystal size (mm)	0.12 × 0.06 × 0.02	0.12 × 0.08 × 0.02	0.18 × 0.03 × 0.01
Crystal system	monoclinic	monoclinic	monoclinic
Space group	*C*2/c	*C*2/c	$P2_1/c$
Temperature (K)	120	120	120
***a* (Å)**	21.3407(14)	33.430(3)	8.9028(6)
***b* (Å)**	15.3842(14)	12.9935(16)	20.1557(12)
***c* (Å)**	21.633(2)	16.4397(19)	15.2276(11)
(º)	90	90	90
(º)	113.749(6)	114.415(5)	98.903(3)
(º)	90	90	90
***V* ($Å^3$)**	6500.9(10)	6502.3(13)	2699.6(3)
Z	4	4	2
(mm^{-1})	0.802	0.759	0.855
$_{min}$ - $_{max}$	1.69° - 24.49°	1.34° - 20.89°	2.02° - 25.45°
Refl. coll. / unique	69168/5382	76581/3419	47326/4976
Completeness to	99.6	99.7	99.5
R_{int}	0.0495	0.0413	0.0688
Refined param./restr.	488 / 0	466 / 72	370 / 0
Goodness-of-fit	1.104	1.098	1.090
[a]R_1 ($I > 2$ (I))	0.0693	0.0596	0.0653
[b]wR_2 (all data)	0.2008	0.1759	0.1629

[a]$R_1 = \Sigma||F_0| - |F_C||/\Sigma|F_0|$ and [b]$wR_2 = [\Sigma w(F_0^2 - F_C^2)^2/\Sigma w(F_o^2)^2]^{1/2}$

Table S2. Relevant bond distances (Å) and intermolecular interactions (Å) in **1 - 3** at 120 K.

	1	**2**	**3**
$d_{arom.}(C_{py}\text{-}C_{py})$ in tphz (Å)[a]	1.390	1.394	1.396
$d(C_{py}\text{-}N_{py})$ in tphz (Å)[a]	1.346	1.350	1.350
d(N2−N2') Å in tphz (Å)	2.758	2.807	2.840
$d_{arom.}(C_{py}\text{-}C_{py})$ in tpy (Å)[a]	1.385	1.379	1.382
$d_{non\text{-}arom.}(C_{py}\text{-}C_{py})$ in tpy (Å)[a]	1.481	1.483	1.479
$d(C_{py}\text{-}N_{py})$ in tpy (Å)[a]	1.343	1.343	1.345
Shortest intermolecular Ni···Ni distance (Å)	9.158	8.795	8.682

3. Spectroscopy

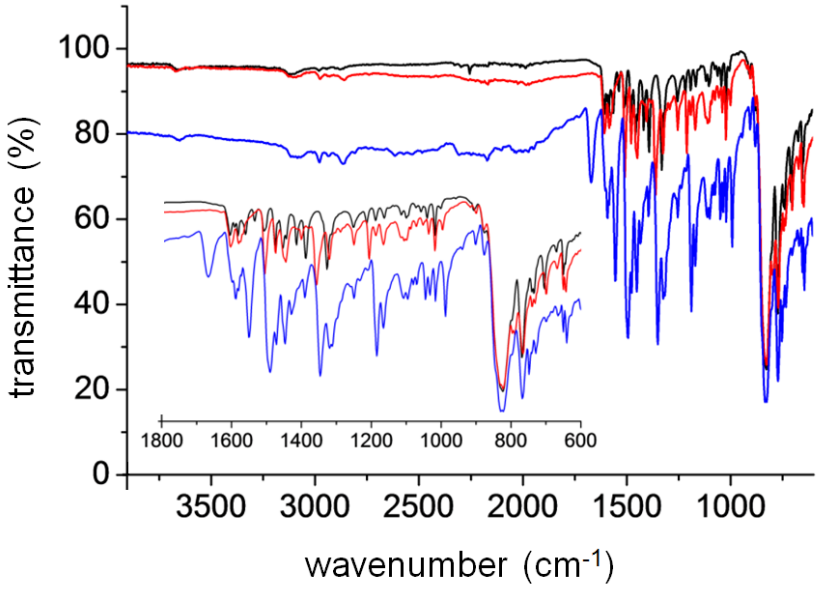

Figure S2. Solid state IR spectra of **1** (black) and **2** (red) and **3** (blue) at room temperature; inset: zoom of the main figure.

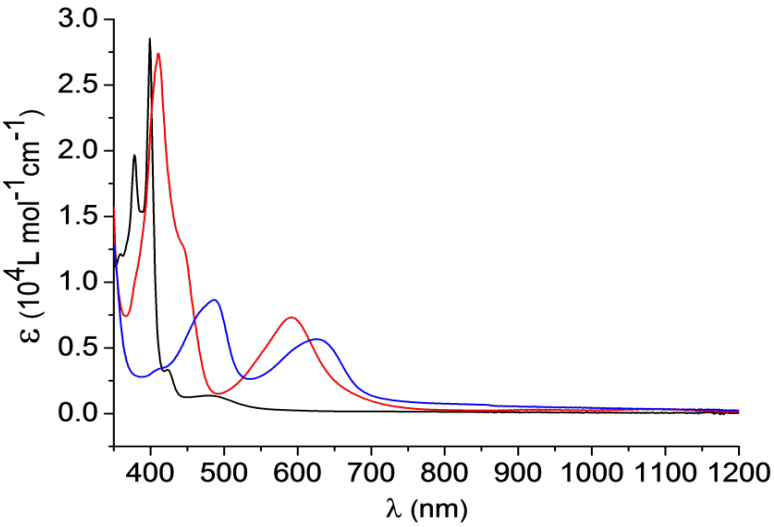

Figure S3. UV/visible/near-IR spectra of **1** (black) and **2** (red) and **3** (blue) in CH_3CN at 298 K.

4. Computational details

The exchange interactions have been computed using the broken-symmetry approach as implemented in ORCA 4.0 with B3LYP/def-TZVP method on the basis of X-ray crystal structures. In the case of two identical spin centers, the broken symmetry solution is an open shell singlet state, which corresponds to a spin flip on one of the sites. The Ni(II) center is assumed to be in its triplet state. The views of the computed spin-density for the three complexes shown in Figure 4 of the main text have been calculated from the broken symmetry solution.

a. Ab initio ligand field analysis.

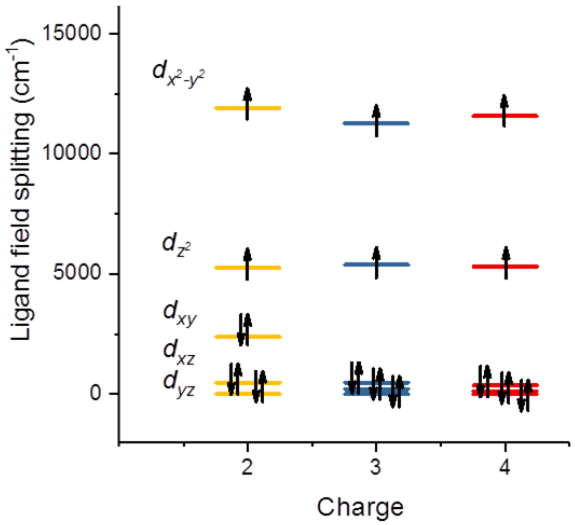

Figure S4. Ligand field splitting for the Ni(II) site in complexes **1** - **3** obtained by ab initio ligand field analysis based on CASSCF calculations. The splitting of *d*-orbitals is characteristic for an elongated octahedron with a large splitting of e_g orbitals and the d_{z^2} orbital that is lower in energy than $d_{x^2-y^2}$ due to the bond lengths to the axial tphz nitrogen atoms (Ni-N1 and Ni-N3; the average N1-Ni-N3 axis is taken as the *z* direction by convention) that are larger than equatorial bond lengths (Ni-N_i; i = 2, 4, 5, 6, see Figure 1).

The ligand field was computed with SOC-CASSCF(8,5)/def2-TZVP method, where 10 triplet and 15 quintet states were mapped onto crystal field Hamiltonian as implemented in ORCA 4.0. For these calculations, one of the Ni(II) sites was substituted with Zn, and the charge for the once reduced compound was kept +4 to ensure that all unpaired electrons are localized on Ni(II).

b. Exchange interaction from broken-symmetry approach.

The exchange coupling constant (*J*) have been computed using the broken-symmetry approach. In the case of two identical spin centers, the broken symmetry solution is an open-shell singlet state, which corresponds to a spin flip on one of the two sites. The exchange coupling constant (*J*) is then computed as:[11]

$$J = -\frac{E_{\mathrm{HS}} - E_{\mathrm{BS}}}{\langle S^2\rangle_{\mathrm{HS}} - \langle S^2\rangle_{\mathrm{BS}}}$$

with E_{HS} and $\langle S^2\rangle_{HS}$ being the energy and the expectation value of the squared spin operator of the maximum multiplicity state, E_{BS} is the energy of the open-shell singlet and $\langle S^2\rangle_{BS}$ its non-zero expectation value. In the case of a three spin system like Ni(II)-radical-Ni(II), there are two different broken-symmetry solutions noted “UDU” for up-down-up, where spin of the radical is flipped compared to the Ni ones, and “UUD” for up-up-down with one of the Ni(II) spins flipped compared to the second Ni and the radical spins. Therefore, the two exchange interactions can be computed as

$$J_{\mathrm{Ni-R}} = -\frac{E_{\mathrm{UUU}} - E_{\mathrm{UDU}}}{\langle S^2\rangle_{\mathrm{UUU}} - \langle S^2\rangle_{\mathrm{UDU}}}$$

$$J_{\mathrm{Ni-Ni}} = -\frac{\frac{1}{2}(E_{\mathrm{UUU}} + E_{\mathrm{UDU}}) - E_{\mathrm{UUD}}}{\frac{3}{4}\langle S^2\rangle_{\mathrm{UUU}} + \frac{1}{4}\langle S^2\rangle_{\mathrm{UDU}} - \langle S^2\rangle_{\mathrm{UUD}}}$$

b.1. Not reduced complex $[Ni_2(tphz)(tpy)_2]^{4+}$ in 1.

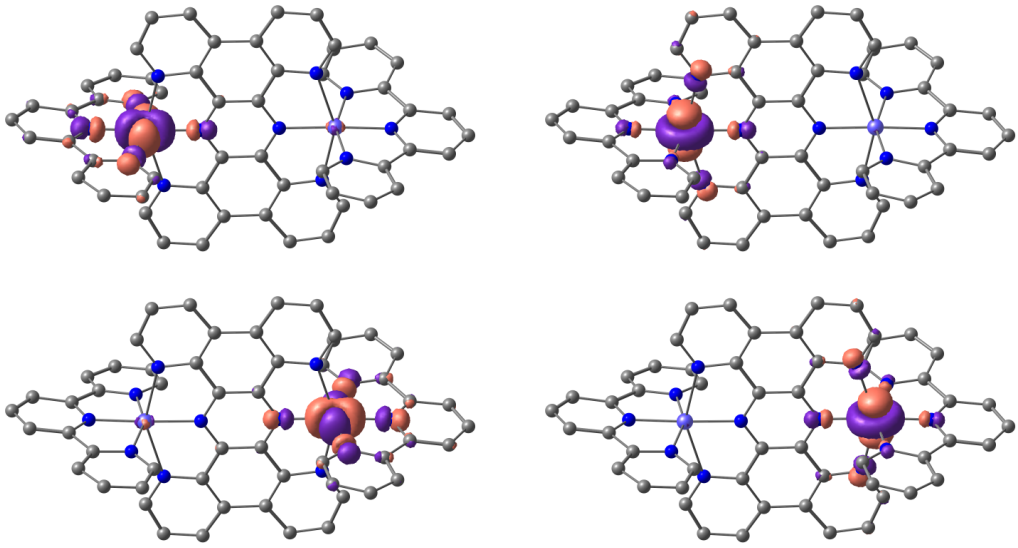

Figure S5. SOMO of $[Ni_2(tphz)(tpy)_2]^{4+}$ in **1** showing the unpaired electrons mainly localized in the $d_{x^2-y^2}$(left) and d_{z^2} (right) orbitals of the Ni sites.

b.2. Once reduced complex $[Ni_2(tphz)(tpy)_2]^{3+}$ in 2.

Table S3. Computed energies and corresponding S^2 expectation values for the different configurations.

Configuration	*E* (a.u.)	$<S^2>$
UUU	-5751.845296	8.7733
UUD	-5751.843736	2.7691
UDU	-5751.842137	4.7649

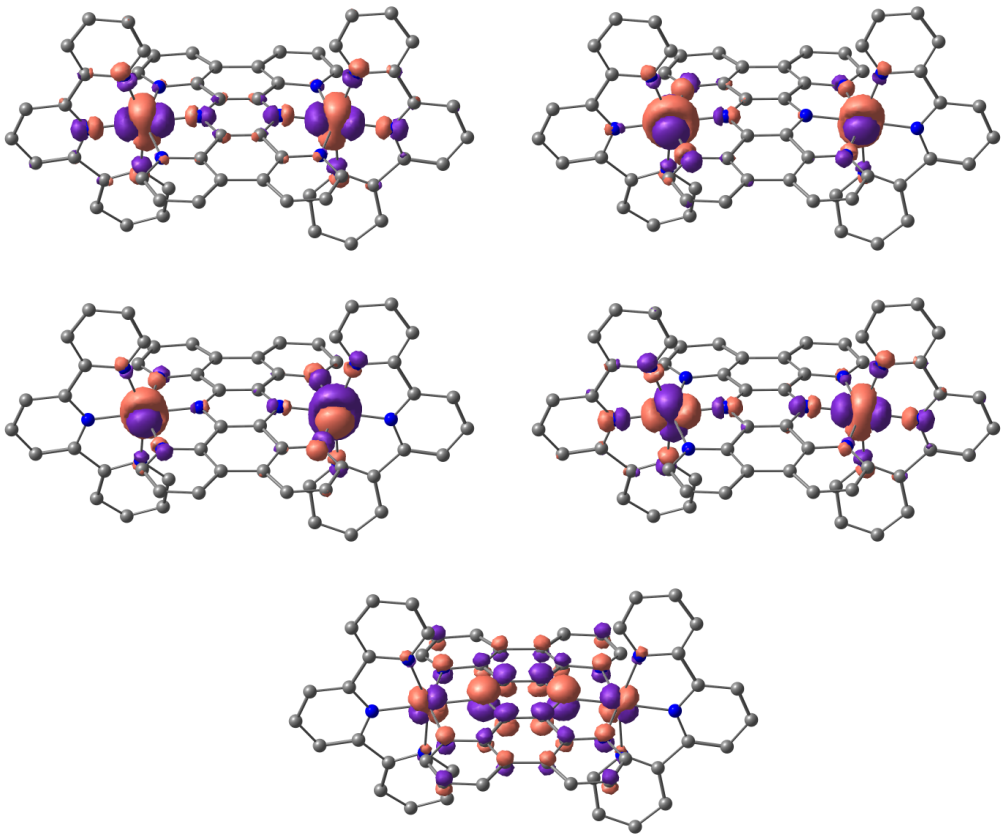

Figure S6. SOMO of $[Ni_2(tphz)(tpy)_2]^{3+}$ in **2**.

b.3. Twice reduced complex $[Ni_2(tphz)(tpy)_2]^{2+}$ in 3.

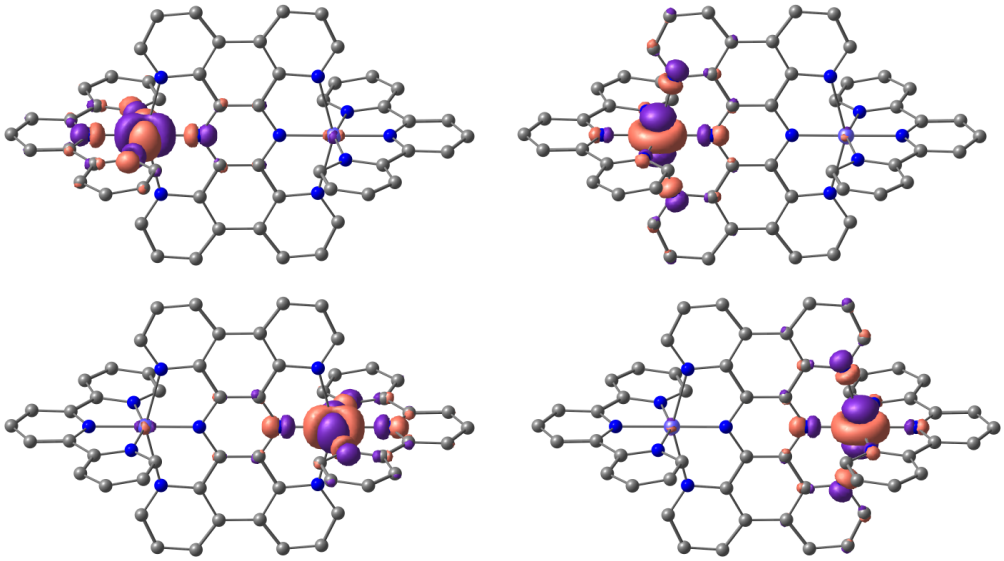

Figure S7. SOMO of $[Ni_2(tphz)(tpy)_2]^{2+}$ in **3** showing the unpaired electrons mainly localized in the $d_{x^2-y^2}$ (left) and d_{z^2} (right) orbitals of the Ni sites. The $d_{x^2-y^2}$ and d_{z^2} orbitals are interacting with σ-orbitals on nitrogen atoms, preventing any spin delocalization.

5. Additional magnetic data

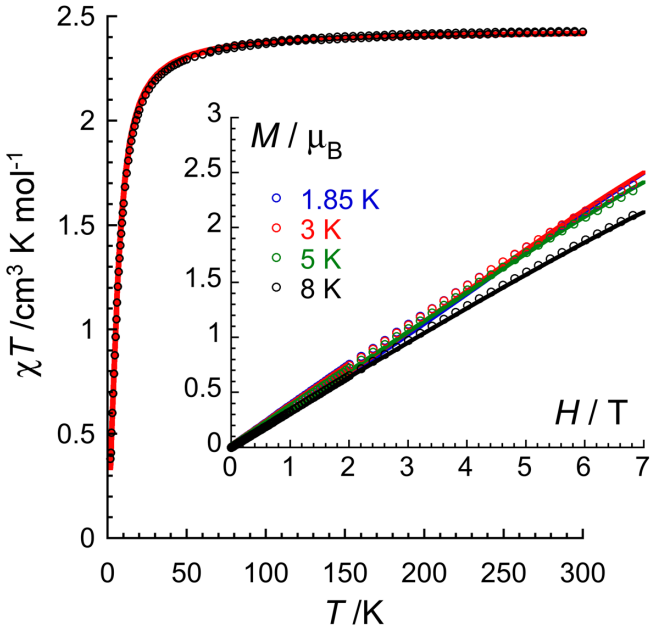

Figure S8. Temperature dependence of the χT product for **1** at 0.1 T. Inset: magnetization versus field curves for **1** below 8 K. The solid lines represent the best fit of the experimental data as discussed in the text with the following Hamiltonian : $\widehat{H} = -2J_{\mathrm{Ni-Ni}}(\vec{S}_{\mathrm{Ni1}} \cdot \vec{S}_{\mathrm{Ni2}}) + 2D_{\mathrm{Ni}}S_{\mathrm{Ni},z}^2 + 2g_{\mathrm{Ni}}\mu_{\mathrm{B}}\vec{S}_{\mathrm{Ni}} \cdot \vec{H}$. The obtained parameters are g_{Ni} = 2.21(5), D_{Ni}/k_B = +13.6(3) K and $J_{Ni\text{-}Ni}/k_B$ = -1.86(3) K.

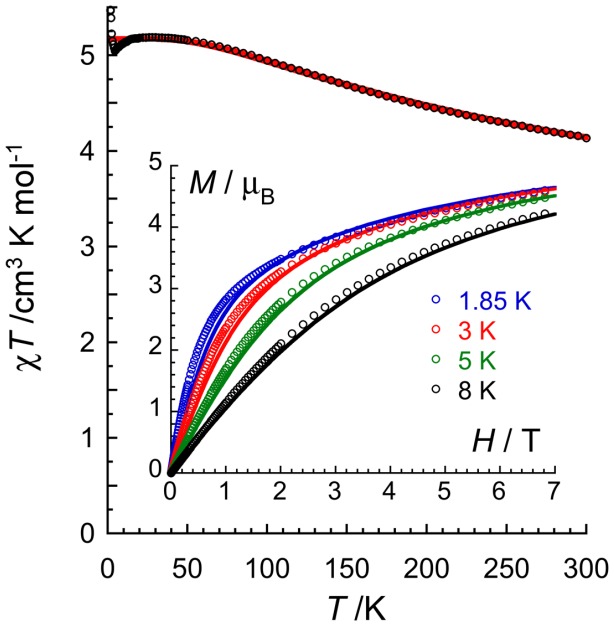

Figure S9. Temperature dependence of the χT product for **2** at 0.1 T. The solid line represents the best fit of the experimental data as discussed in the text based on the following Hamiltonian: $\widehat{H} = -2J_{\mathrm{Ni-rad}}\left(\vec{S}_{\mathrm{Ni1}} + \vec{S}_{\mathrm{Ni2}}\right) \cdot \vec{S}_{\mathrm{rad}} + \mu_{\mathrm{B}}\left(2g_{\mathrm{Ni}}\vec{S}_{\mathrm{Ni}} + g_{\mathrm{rad}}\vec{S}_{\mathrm{rad}}\right) \cdot \vec{H}$ with g_{rad} fixed at 2, the obtained parameters are g_{Ni} = 2.20(5) and $J_{\mathrm{Ni\text{-}rad}}/k_{\mathrm{B}}$ = +214(5) K. Inset: magnetization versus field curves for **2** below 8 K. The solid lines correspond to the best fit of the experimental to an S_{T} = 5/2 macrospin model with the following Hamiltonian: $\widehat{H} = DS_{\mathrm{T,z}}^2 + E\left(S_{\mathrm{T},x}^2 - S_{\mathrm{T},y}^2\right) + g\mu_{\mathrm{B}}\vec{S}_{\mathrm{T}} \cdot \vec{H}$. The obtained parameters are g = 2.17(5), D/k_{B} = +3.9(1) K and E/k_{B} = +0.79(4) K.

It is worth noting that at low temperatures (below 20 K), Ni magnetic anisotropy and inter-complex magnetic interactions are competing as observed by the thermal behavior of the χT product between 18 and 1.85 K. The effects of the Ni(II) magnetic anisotropy on the χT vs T data are clearly seen by the slight χT decrease between 18 and 4 K, while at lower temperatures, the χT increase highlights the presence of weak effective ferromagnetic inter-molecular interactions between complexes.

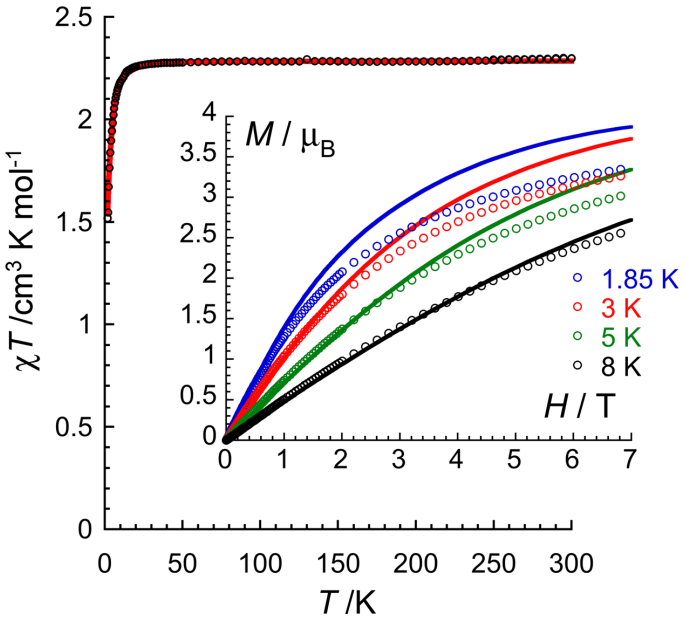

Figure S10. Temperature dependence of the χT product for **3** at 0.1 T. Inset: magnetization versus field curves for **3** below 8 K. The solid lines represent the best fit of the experimental data as discussed in the text with the following Hamiltonian: $\hat{H} = D_{\mathrm{Ni}} S_{\mathrm{Ni},z}^2 + g_{\mathrm{Ni}} \mu_{\mathrm{B}} \vec{S}_{\mathrm{Ni}} \cdot \vec{H}$. The obtained parameters are g_{Ni} = 2.14(5) and $D_{\mathrm{Ni}}/k_{\mathrm{B}}$ = -10.4(3) K when $J_{\mathrm{Ni\text{-}Ni}}/k_{\mathrm{B}}$ is fixed to zero. The addition of a Ni-Ni magnetic coupling in the model does not improve the fit, leading systematically to extremely small value of $J_{\mathrm{Ni\text{-}Ni}}/k_{\mathrm{B}}$ ($|J_{\mathrm{Ni\text{-}Ni}}/k_{\mathrm{B}}|$ < 0.1 K).

6. References

[1] G. M. Sheldrick, SADABS Version 2.03, Bruker Analytical X-Ray Systems, Madison, WI, USA, 2000.

[2] G. M. Sheldrick, *Acta Cryst.* **2015**, C*71*, 3-8.

[3] A. L. Spek, *Acta Cryst.* **2015**, C*71*, 9-18.

[4] F. Neese, *WIREs Comput. Mol. Sci.* **2012**, *2*, 73-78.

[5] M. Atanasov, D. Ganyushin, K. Sivalingam, F. Neese, *A Modern First-Principles View on Ligand Field Theory Through the Eyes of Correlated Multireference Wavefunctions.* In: D. Mingos, P. Day, J. Dahl (eds) Molecular Electronic Structures of Transition Metal Complexes II. *Structure and Bonding*, **2011**, 143. Springer, Berlin, Heidelberg.

[6] D. Ganyushin, F. Neese, *J. Chem. Phys.,* **2013**, *138*, 104113.

[7] P. Bonhôte, A. Lecas, E. Amouyal, *Chem. Commun.* **1998**, *8*, 885-886.

[8] P. Bonhôte, M. S. Wrighton, *Synlett.* **1997**, 897-898.

[9] D. M. D'Alessandro, F. R. Keene, *Dalton Trans.* **2006**, *8*, 1060-1072.

[10] F. Lions, I. G. Dance, J. Lewis, *J. Chem. Soc. A*, **1967**, 565-572.

[11] (a) K. Yamaguchi, Y. Takahara, T. Fueno in *Applied Quantum Chemistry*. V. H. Smith (Ed.), Reidel, Dordrecht (1986), pp 155; (b) T. Soda, Y. Kitagawa, T. Onishi, Y. Takano, Y. Shigeta, H. Nagao, Y. Yoshioka, K. Yamaguchi. *Chem. Phys. Lett.*, **2000**, 319, 223-230.